Two-Frequency Electron Spin Echo Envelope Modulation and Electron Spin Echo Decay of Cu(II)−(Alkylthio)tetraazaporphyrin Powder

M. Romanelli* and F. Bonosi

Dipartimento di Chimica, Universita' di Firenze, 50121 Firenze, Italy

V. Kurshev† and L. Kevan

Department of Chemistry, University of Houston, Houston, Texas 77204-5641

Received: April 17, 1995⊗

Electron spin echo signals from a powder sample of Cu(II)−(alkylthio)tetraazaporphyrin diluted in the corresponding Ni(II) compound are analyzed. The electron spin echo envelope modulation is analyzed to determine the structural arrangement around the paramagnetic center, and the electron spin echo decay is studied to obtain information on the electron spin relaxation mechanism. This information is of help in elucidating the structure and properties of Langmuir−Blodgett films fabricated by the title material. The experiments were run both at X-band (9.8 GHz) and at S-band (2.7 GHz), and the experimental spectra were interpreted by best-fit procedures with computed patterns in the time domain.

Introduction

(Alkylthio)tetraazaporphyrin compounds of Cu(II) (Cu−TAP) have been recently used as materials to build up thin films as spread monolayers and as Langmuir−Blodgett films. They form discotic liquid crystals as columnar aggregates that are stable over a wide range of temperatures.[1−5] This feature, if maintained in thin films, can help in forming Langmuir−Blodgett films with unusual conductive and reactive properties. Since it has been shown that the molecular ordering increases in the presence of hydrophobic and hydrophilic chains,[6−8] compounds with approprite chain substituents have also been synthesized.[9] Information on the molecular structure and dynamics can help in the elucidation of the properties exhibited by these materials. Thus, we have applied the electron spin echo (ESE) technique to investigate intramolecular interactions in these compounds as well as their intermolecular interactions.

The ESE experiments were run at X-band (~9 GHz) and S-band (~3 GHz) at different temperatures on a typical Cu-TAP compound diluted in the corresponding Ni-TAP compound to avoid spin−spin interactions. The study was carried out on the compound with no chain substitutions, because it has simpler symmetry and has been characterized more extensively than the substituted compounds.[3]

Two microwave frequencies were used because the additional constraints in fitting data at two frequencies can reduce any ambiguity in the determination of the spectral parameters by best-fit simulation procedures. Moreover, S-band ESE has been useful to detect the presence of nuclei giving weak echo modulation at X-band because of a long interaction distance with the paramagnetic center. Theory predicts that the nuclear modulation amplitude is inversely proportional to the square of the nuclear Larmor frequency; this prediction has been experimentally confirmed.[10−12] From the analysis of the electron spin echo envelope modulation (ESEEM), we obtained information on the structural arrangement of the magnetic nuclei around the paramagnetic center. The interpretation of the electron spin echo signal decay as a function of the temperature determines the relaxation rate over 4−70 K and helps to determine the electron relaxation mechanism.

Experimental Section

The metal−(alkylthio)tetraaza compounds 2,3,7,8,12,13,17,18-octakis(octylthio)-5,10,15,20-tetraazaporphyrin (Scheme 1) were prepared as reported.[5] The Cu(II) compound, used for fabrication of Langmuir−Blodgett films, was diluted with the corresponding Ni(II) compound in an atomic ratio of 1:100. The two-pulse and three-pulse ESE experiments were run in the temperature range 4−70 K on a commercial Bruker ESP-380 (X-band) spectrometer and on a laboratory-designed pulsed spectrometer (S-band) described elsewhere.[11] The two-pulse and three-pulse sequences at X-band were (24−τ−48 ns) and (24−τ−24−T−24 ns), respectively. The first interpulse time τ in the three pulse sequence was kept constant at 360 ns. S-band patterns were obtained by (30−τ−60 ns) two-pulse sequences and (30−τ−30−T−30 ns) three-pulse sequences, where τ = 500 ns.

Computation Procedure

The analysis of the experimental patterns is carried out by best fit with simulated patterns, where both the decay and the nuclear modulation of the electron spin echo signal are taken into account. The overall echo signal $E(t)$ is calculated by eq 1:

$$E(t) = D(t)\, V(t) \tag{1}$$

The computation of the overall nuclear modulation function $V(t)$ was carried out on the basis of the modulation product rule[13] in (2)

$$V(t) = \prod_{i=1}^{n} V_i(t) \tag{2}$$

where n is the number of nuclei contributing to the overall

† On leave from the Institute of Chemical Kinetics and Combustion, Novosibirsk 630090, Russia.

⊗ Abstract published in *Advance ACS Abstracts,* July 15, 1995.

0022-3654/95/2099-12597$09.00/0

SCHEME 1

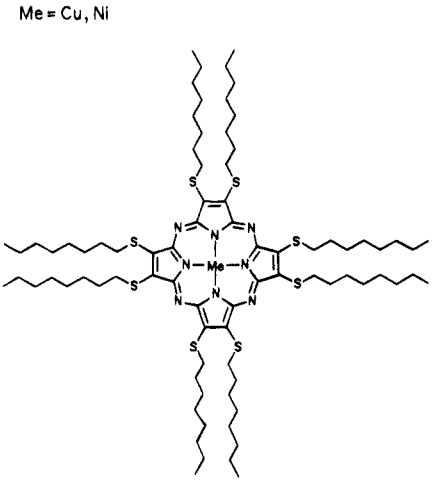

modulation. In our case we can write (3)

$$V(t) = \prod_{i=1}^{m} V_{H,i}(t) \prod_{h=1}^{s} V_{N,h}(t) \tag{3}$$

where V_H and V_N indicate the nuclear modulation due to protons and to nitrogens, respectively. Due to the large nitrogen nuclear quadrupole moment, V_N was computed by numerical diagonalization of the nuclear Hamiltonian matrices. V_H was computed by exact analytical equations for a $S = {}^1/_2$, $I = {}^1/_2$ spin system:[14]

$$V(2\tau) = 1 - 2k \sin^2 \pi\nu_\alpha\tau \sin^2 \pi\nu_\beta\tau$$

$$V(2\tau+T) = 1 - k[\sin^2 \pi\nu_\alpha\tau \sin^2 \pi\nu_\beta (\tau+T) + \sin^2 \pi\nu_\beta\tau \sin^2 \pi\nu_\alpha(\tau+T)] \tag{4}$$

The presence of few nuclei at relatively short distance ($r \leq 0.36$ nm) from a paramagnetic center with a large **g**-tensor anisotropy requires an ESEEM computation by a procedure that takes partial excitation into account. By defining a molecular axis system with the z-axis parallel to $g_{\parallel}$ and the x-axis parallel to $g_{\perp}$, we used the approach developed by Anderson and Kevan[15] to calculate the averaged modulation due to n nuclei by eq 5:

$$\langle V \rangle^n = \left\{ \frac{1}{2\pi \sin \theta_0{}^c \sin \delta} \int_0^{2\pi} \int_{\theta_0{}^c-\delta}^{\theta_0{}^c+\delta} V(\theta_I,\theta_0,\phi_I) \sin \theta_0 \, d\theta_0 \, d\phi_I \, d\theta_I \right\}^n \tag{5}$$

with $\theta_0{}^c$ the value of the polar angle between the z-axis and B_0. 2δ is the range of θ_0 covered by the pulse width, so that $(\theta_0{}^c - \delta) \leq \theta_0 \leq (\theta_0{}^c + \delta)$. θ_I is the angle between z and the electron–nucleus distance vector **r**. ϕ_I is the azimuthal angle between the zx plane and the zB_0 plane.

For n nuclei located at long distances ($0.36 \leq r \leq 0.7$ nm) we applied the spherical approximation (6):[16]

$$\int_\Omega d\Omega \prod_{h=1}^{n} V_N(\theta,\phi)_h = [\int_\Omega V_N(\theta,\phi) \, d\Omega]^n \tag{6}$$

The modulation due to nuclei at $r > 7$ nm was computed by the approach developed by Mims[17] for a continuous distribution of nuclei.

The decay function $D(t)$ was evaluated on the basis of equations involving the concentration C_A of A-spins (the spins rotated by the microwave pulses), the concentration C_B of B-spins (the remainder of spins in the system), and the spin reorientation time τ_r (the time characterizing the relaxation mechanism). Both the instantaneous diffusion[18] and spectral diffusion mechanisms were taken into account.

In the Mims model[19] where the correlation function of the z-projection of the spins is described by a normal Gaussian process, the echo decay in the two-pulse and three-pulse sequences when $(\tau,T) > \tau_r$ is described by eq 7.

$$D(2\tau) = D(2\tau+T) = D_0 \exp\{-1.1[\Delta\omega_B + \Delta\omega_A]\sqrt{2\tau_r\tau}\} \tag{7}$$

T indicates the second interpulse time in the three-pulse sequence to distinguish it from the temperature T. When $(\tau,T) < \tau_r$, the echo signal decays in the two-pulse sequence as in (8):

$$D(2\tau) = D_0 \exp\left\{-1.1\left[\Delta\omega_B\sqrt{\frac{2\tau^3}{3\tau_t}} + \Delta\omega_A\sqrt{2\tau^2 - \frac{4\tau^3}{3\tau_r}}\right]\right\} \tag{8}$$

and in the three-pulse sequence as in (9):

$$D(2\tau+T) = D_0 \exp\left\{1.1\left[\Delta\omega_B\tau\sqrt{1 - \exp\left(-\frac{T}{\tau_r}\right)} + \Delta\omega_A\sqrt{0.5\tau^2\left(1 - \frac{\tau}{3\tau_r}\right)}\right]\right\} \tag{9}$$

In the above formula D_0 is a normalization constant, and $\Delta\omega_{A,B}$ is the ESR line width related to the B-spin and A-spin concentrations:

$$(4\pi^2/9\sqrt{3})\gamma_A\gamma_B\hbar C_{A,B} \tag{10}$$

The first step of the best-fit procedure was the evaluation of the modulation function for the protons and nitrogens on the basis of the X-band three-pulse experimental pattern at 4 K. The same set of parameters was then used to fit the corresponding experimental pattern at S-band. Then multiplication by the appropriate decay function (see Decay Function section) was carried out. Finally, refinement of the modulation function parameters was performed until the best fit with the two-pulse patterns at both X-band and S-band was attained.

Results and Discussion

Nuclear Modulation. Figure 1 shows the experimental (full line) X-band three-pulse (a) and two-pulse (b) patterns of Cu–TAP diluted 1:100 in Ni–TAP at 4 K. Pure Cu–TAP gave no echo due to strong spin–spin interactions that caused fast signal decay. Figure 2 shows the two-pulse pattern of the same sample at S-band at 4 K. All the patterns exhibit a dominant modulation due to protons in the alkyl chains. An underlying modulation due to the noncoordinated ^{14}N is also present (the coordinated nitrogens do not give nuclear modulation due to their large hyperfine coupling[20]), which is more evident in the X-band patterns.

Structural data indicate that the four imidazole rings lie on the same plane.[21] From a simple molecular model, in this arrangement the four noncoordinated nitrogens are on the same plane at 0.36 nm from the central ion, and there are 16 closest alkyl protons on the carbons adjacent to the sulfur at distance $0.66 < r < 0.7$ nm from the central ion. To evaluate the V_H of this set of protons, it is appropriate to use the exact analytical

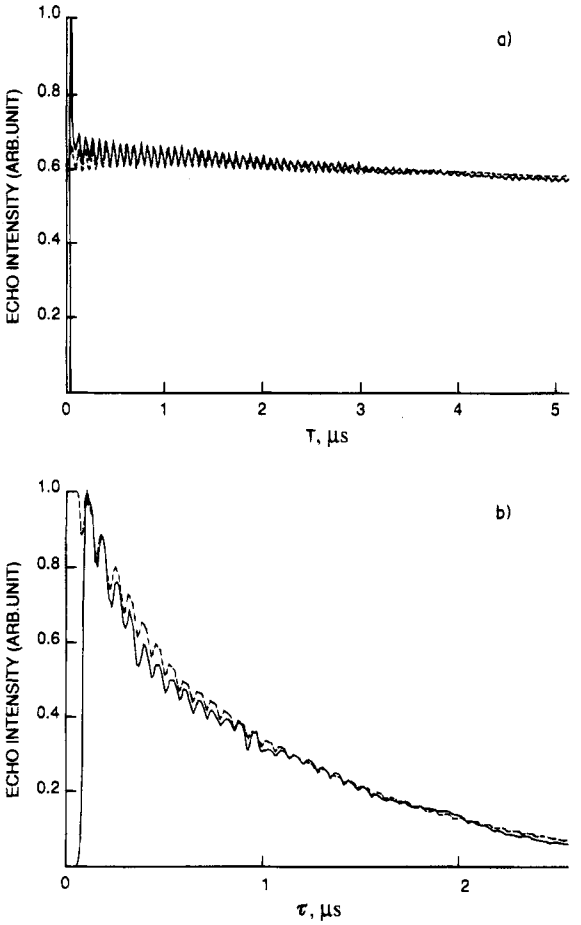

Figure 1. X-band (9.85 GHz) electron spin echo signals of Cu−TAP 1:100 in Ni−TAP at 4 K: (a) three-pulse experimental (full line) and best-fit simulated (dashed line) patterns; (b) two-pulse experimental (full line) and best-fit simulated (dashed line) patterns. $B_0 = 3370$ G. The ESEEM and electron spin echo decay best fit parameters are in Tables 1 and 2, respectively.

equations (4). A method to calculate the contribution to the overall modulation by the remainder of the alkyl protons is to multiply seven contributions at different distances, each contribution being determined by a spherical distribution of 16 protons. However, at these long distances the overall modulation is not very sensitive to the value of the distance chosen for each sphere. Moreover, one has to take into account that also protons belonging to chains of other nearest molecules can contribute to the overall modulation. It seemed thus more appropriate to evaluate the proton overall modulation as due to the 16 nearest protons and to a continuous proton distribution beyond them beginning from $r = 7$ nm. The density of protons in the continuum was evaluated as $\varrho_H = 200$ spin/nm^3, from the sample density of 2.5 g/cm^3.

The simulation of the proton modulation with these parameters was in agreement with the long-time behavior ($\tau > 0.5$ μs, $T > 1$ μs) of the experimental modulation, but it did not reproduce the deep proton modulation present at short τ values in the experimental two-pulse pattern at X-band that is characteristic of closer protons. This requirement was confirmed by the shape of the proton modulation at S-band (Figure 2), where the second peak of the indentation due to the $2\omega_H$ component is higher than the first one. These experimental features can be reproduced in the simulations by introducing protons at shorter distances ($r < 0.66$ nm). This requires the use of eq 5.

To carry out this approach, it is necessary to know the g-tensor components and the range of the polar angle θ_0 covered

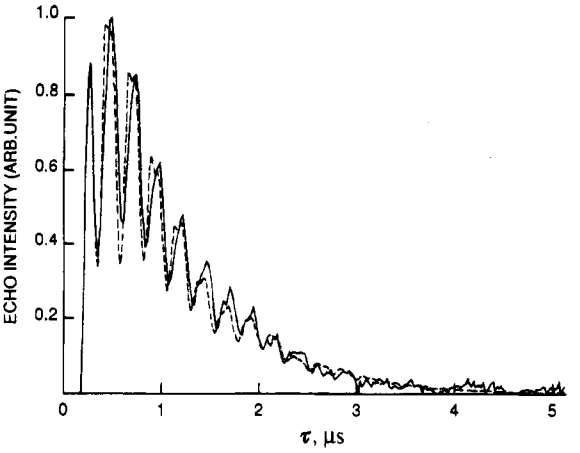

Figure 2. S-band (2.68 GHz) two-pulse experimental electron spin echo signal of Cu−TAP 1:100 in Ni−TAP at 4 K (full line) and best-fit simulated (dashed line) pattern. $B_0 = 985$ G. ESEEM and electron spin echo decay best fit parameters are in Tables 1 and 2, respectively.

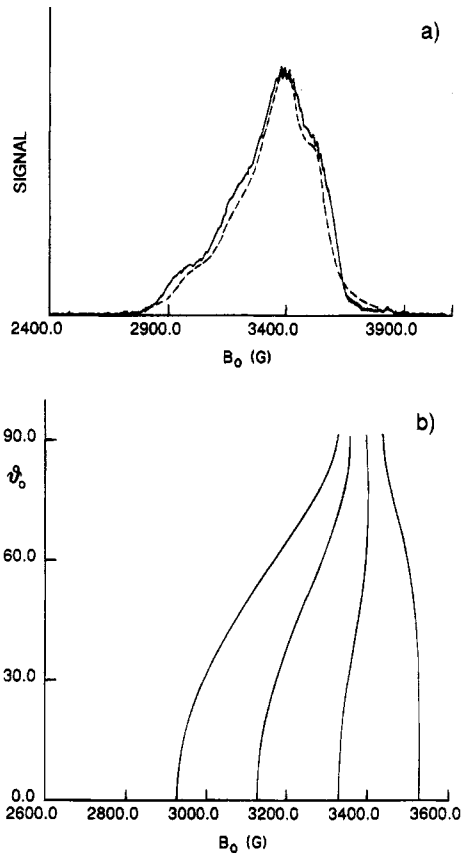

Figure 3. (a) Comparison between the X-band ESR experimental absorption (full line) at 4 K of Cu−TAP 1:100 in Ni−TAP and the computed spectrum with best-fit parameters $g_{||} = 2.170$, $g_\perp = 2.065$, $A_{||} = 200$ G, and $A_\perp = 37$ G. Lorentzian spin packets with a line width of $\delta B = 45$ G were used for simulation. (b) Behavior of the four hyperfine transitions as a function of the polar angle θ_0 (see text).

by the width of the microwave pulse. The evaluation of the g-tensor components was done by simulating the ESR absorption pattern using spin packets with Lorentzian line shapes. The best fit with the experimental spectrum, shown in Figure 3a, was obtained with $g_{||} = 2.170$, $g_\perp = 2.065$, $A_{||} = 200$ G, $A_\perp = 37$ G, and a line width of a spin packet of $\delta B = 45$ G. In the computed spectrum the superhyperfine structure due to the nearest nitrogens was neglected. The behavior of the four hyperfine transitions as a function of θ_0 calculated by using the best-fit g and A components is shown in Figure 3b. At $B_0 = 3370$ G, $\theta_0^c = 62.2°$; since our pulse width amounts to 7 G,

TABLE 1: Parameters[a] That Give the Best-Fit Modulation Function $V(t)$

nucleus	X-band	S-band
^{1}H	$n_1 = 2$, $r_1 = 0.38$, $\theta_l = 40°$ $n_2 = 8$, $r_2 = 0.60$ $n_3 = 16$, $r_3 = 0.66$ continuous distribution beyond $r = 0.7$ nm ($\varrho_H = 200$ spin/nm^3)	$n_1 = 2$, $r_1 = 0.38$, $\theta_l = 40°$ $n_2 = 8$, $r_2 = 0.60$ $n_3 = 16$, $r_3 = 0.66$ $n_4 = 16$, $r_4 = 0.82$ continuous distribution beyond $r = 0.9$ nm ($\varrho_H = 200$ spin/nm^3)
^{14}N	$n = 4$, $r = 0.36$ $a_{iso} = 0.1$, $Q = 0.5$	$n = 4$, $r = 0.36$ $a_{iso} = 0.1$, $Q = 0.5$

[a] n_i and r_i are the number and distance of nuclei in the ith set; r in nm, a_{iso} and Q in MHz.

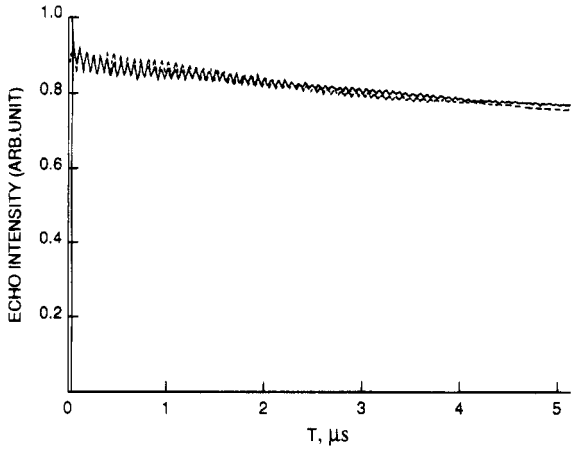

Figure 4. X-band experimental (full line) three-pulse pattern at 20 K of Cu-TAP 1:100 in Ni−TAP and best-fit simulated pattern (dashed line). The ESEEM and electron spin echo decay best fit parameters are in Tables 1 and 2, respectively.

$\delta = 3.1°$ is the value to be used in the integration of eq 5. The sets of parameters that give the best fit for the proton modulation at both the frequencies are shown in Table 1. Both the X-band and S-band data indicate three sets of protons, with two protons located 0.38 nm from the paramagnetic center, eight protons located 0.60 nm away, and 16 protons located 0.66 nm away. The presence of the protons at $r = 0.38$ nm and $r = 0.60$ nm can be interpreted in different ways. If they belong to the same molecule, one has to assume that one or two alkyl chains undergo a sharp bend. If an extended arrangement of the alkyl chains occurs, the additional protons at 0.38 nm can belong either to chains of surrounding molecules or to solvent molecules (dichloroethane or chloroform) that are not completely removed. The 16 protons at $r = 0.66$ nm can be identified as the closest set of protons of the alkyl chains of the molecule. The S-band best-fit parameters differ from those of X-band by a discrete contribution due to 16 protons at 0.82 nm and by the longer distance at which the continuum begins. This is consistent with the expected sensitivity at S-band for protons at longer distances. Even if the number is not so critical, this difference seems indicate an extended arrangement of the alkyl chains up to the second carbon.

The modulation $V_N(t)$ due to the four noncoordinated nitrogens was computed by eq 5 with $r = 0.36$ nm. In this case, the input trial parameters were the isotropic hyperfine constant a_{iso} and the nuclear quadrupole coupling Q.

In Table 1 the best-fit magnetic parameters are reported. They were determined by a combined analysis of the X-band and S-band two-pulse patterns. The modulation at S-band is more sensitive to changes of the nuclear quadrupole coupling and of the isotropic hyperfine coupling because the nuclear Zeeman interaction is weaker than at X-band. Indeed, changing

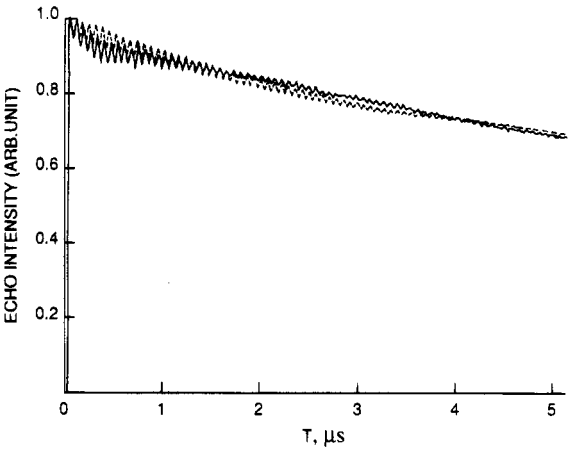

Figure 5. X-band experimental (full line) three-pulse pattern at 50 K of Cu−TAP 1:100 in Ni−TAP and best-fit simulated pattern (dashed line). ESEEM and electron spin echo decay best fit parameters are in Tables 1 and 2, respectively.

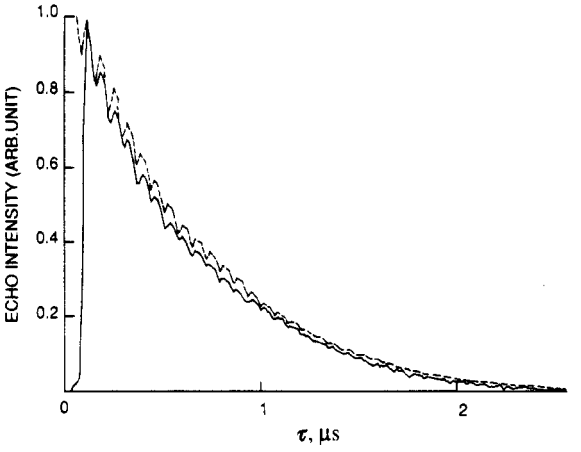

Figure 6. X-band experimental (full line) two-pulse pattern at 70 K of Cu−TAP 1:100 in Ni−TAP and best-fit simulated pattern (dashed line). ESEEM and electron spin echo decay best fit parameters are in Tables 1 and 2, respectively.

a_{iso} in the range 0.1−0.4 MHz and Q in the range 0.3−0.5 MHz gave X-band modulations that fit reasonably with the experiments, so that some ambiguity exists in assigning a best set of parameters to the nitrogens. In contrast, simulations at S-band with the same sets of parameters as at X-band led to modulations that differ remarkably from each other. The best-fit for the entire set of magnetic parameters is $a_{iso} = 0.1$ MHz and $Q = 0.5$ MHz, as shown in Table 1.

Decay Function. The X-band, three-pulse experimental pattern of Cu−TAP 1:100 in Ni−TAP at 4 K (Figure 1a) exhibits almost no decay over the T range. This behavior characterizes a spectral diffusion mechanism with a long spin reorientation time $\tau_r \gg (T,\tau)$. Indeed, at $\tau_r \gg T$ the reorientation of the B-spins has no effect on the decay and the A-spins contribute only by the instantaneous diffusion occurring during τ. In other words, $D(2\tau+T)$ becomes a constant, and the only information that can be deduced is $\tau_r \gg T$.

In the corresponding two-pulse pattern of Figure 1b, one observes a noticeable signal decay. From eq 8 one finds that at $\tau_r \gg \tau$ the contribution of the B-spin reorientation induces a small effect on the decay, whereas the A-spins contribute mainly by the instantaneous diffusion mechanism. A quantitative extimate of $D(2\tau)$ on the basis of eq 8 requires the knowledge of τ_r, C_A, and C_B. To determine reasonable values of these input parameters, the following considerations were made.

Due to the low concentration of unpaired spins in this sample,

it is reasonable to assume that spin−lattice relaxation is the dominant relaxation mechanism. In this case, τ_r can be identified as T_1. We have no independent experimental measurements of T_1. However, its value can be estimated by equations found to hold for relaxation processes (direct, Orbach, and Raman) in the solid state. Since T_1 exhibits different dependencies on the temperature and on the field B_0 in the different relaxation processes, we ran ESE experiments at different temperatures to ascertain which relaxation process is effective in our sample. In Figures 4, 5, and 6 two- and three-pulse experimental patterns at different temperatures are shown. For the three relaxation processes the equations hold:[22]

$$T_1^{-1} = A\nu_0^3 \coth(\nu_0/2kT) \quad \text{(direct)} \tag{11}$$

$$T_1^{-1} = C\left\{\frac{kT}{h}\right\}^9 I_8 \quad \text{(second-order Raman)} \tag{12}$$

$$T_1^{-1} = B[\exp(\Delta/kT) - 1] \quad \text{(Orbach)} \tag{13}$$

In the above equations A, C, and B are factors depending on the density d of the sample, on the sound velocity v, on the energy gap Δ between the ground and the excited state, and on the potential Φ. ν_0 is the resonance frequency. I_8 is the integral

$$I_8 = \int_0^{\theta_D/T} \frac{x^8 e^x}{(e^x - 1)^2}\,dx \tag{14}$$

with $x = \Delta/kT$ and θ_D the Debye temperature of the sample.

Simulations to fit the decay of the patterns in Figure 1b (X-band) and in Figure 2 (S-band) on the basis of the frequency dependence of T_1 for the direct process were unsuccessful. By considering also that the direct process is effective only at very low temperatures, we discarded this process as determining the relaxation mechanism in our sample. On the other hand, in a Raman process the temperature dependence of $T_1 \propto T^{-9}$ or T^{-7} causes a difference in the T_1's between 20 and 50 K of more than 3 orders of magnitude. Comparison between the three-pulse experimental patterns at 20 and 50 K shown in Figures 4 and 5, respectively, clearly rules out such a strong difference. Thus, we are left with the Orbach process, where T_1 exhibits an exponential dependence on the temperature. This conclusion is in agreement with experimental studies of the relaxation mechanism of Cu(II) ion in sulfuric acid solution.[23] As outlined by Atkins,[24] an Orbach process can involve an electronic or a vibrational state as an excited state separated by energy Δ form the ground state. However, in the latter case (direct vibrational process), T_1 exhibits a dependence on the squared magnetic field as in the direct process and has to be discarded for the same reason.

In the remaining Orbach process, T_1^{-1} is given by[25]

$$T_1^{-1} = \frac{6\lambda^2 h\Delta}{v^5 d}\Phi^2[e^{h\Delta/kT} - 1]^{-1} \tag{15}$$

where λ is the spin−orbit coupling constant. The above equation holds if $\omega_0 < 2\pi\Delta < kT/\hbar$, i.e., at T = 4 K: $9 \times 10^9 < \Delta < 8.4 \times 10^{10}$ s^{-1}. Values of Δ in this range have been found for Ti^{3+}.[26] This condition induces a slowly changing exponential factor in the 20−70 K range that fits the decay behavior of our experimental patterns.

The potential Φ is difficult to be evaluate: reasonable estimates lie in the range $\Delta/10 < \Phi < \Delta/3$.[22,25] By using $\lambda = 2.3 \times 10^{13}$ s^{-1}, $v = 3 \times 10^5$ cm/s, and $d = 2.5$ g/cm^3, simulations were run by varying the C_A and C_B parameters under the constraints due to the experimental conditions: $(C_A + C_B) \leq 2 \times 10^{-2}$ mol/L and $C_A \ll C_B$. Simulations with $\Phi = \Delta/3$ gave T_1 too short to fit the experimental patterns. The best fit was obtained for the overall temperature range with $\Delta = 5 \times 10^{10}$ s^{-1} and $\Phi = \Delta/17$. In Table 2 the best-fit parameters for the decay are reported, and in Figures 4, 5, and 6 the agreement between the X-band experimental and simulated two- and three-pulse patterns is shown. One has to note that at S-band (Figure 2) at 4 K the agreement between the experimental and simulated decay is reached by using the same T_1 as at X-band; this confirms that the relaxation processes involving a dependence of T_1 on the operating frequency are not effective in the relaxation mechanism for this system.

TABLE 2: Parameters That Give the Best-Fit Decay Functions $D(t)$

T (K)	τ_r (μs)	C_B (mol/L)	C_A (mol/L)
4	550	1.0×10^{-2}	1.0×10^{-3}
20	88	0.7×10^{-2}	6.0×10^{-4}
30	58	0.7×10^{-2}	5.0×10^{-4}
50	33	0.73×10^{-2}	4.0×10^{-4}
70	20	0.88×10^{-2}	4.0×10^{-4}

The values of the C_A parameter reported in Table 2 need some critical consideration. They are estimated by simulating the contribution of the A-spins both to the "normal" spectral diffusion and to the instantaneous diffusion mechanisms. An exact evaluation of the latter requires knowledge of the spin resonance frequency distribution to perform the averaging of the angular factors $\langle\cos^2\theta\rangle_\omega$ and $\langle\cos\theta\rangle_\omega$,[27] where θ is the angle through which the A-spins are rotated by the microwave pulses. Our data do not give such information, so we set these factors at their maximum value in all the simulations. This approximation does not take into account of the possible changes of the frequency distribution due to changing temperature, and the changes in C_A with temperature can be caused by this approximation. The small increase of C_B with temperature may be attributed to an increased efficiency of the relaxation process to involve more spins in the spectral diffusion mechanism when temperature increases.

Conclusions

The combined analysis of the ESEEM at X-band and S-band at different temperatures indicates that the interaction of the noncoordinated nitrogens of Cu−TAP with the unpaired electron are characterized by weak isotropic hyperfine and nuclear quadrupole interactions. Moreover, the best-fit parameters of the proton modulation seem indicative of extended alkyl chains up to the second alkyl carbon. The analysis of the electron spin echo decay at different temperatures leads to a spin−lattice relaxation mechanism determined by an Orbach process. The relaxation is affected by the spin concentration, and both the instantaneous diffusion due to A-spins and normal spectral diffusion play a role in determining the echo decay at different temperatures.

Acknowledgment. This research was supported by the National Science Foundation, the Robert A. Welch Foundation, the U.S. Department of Energy, and the Italian Ministero dell' Universita' e della Ricerca Scientifica (MURST) and the Italian Consiglio Nazionale delle Ricerche (CNR).

References and Notes

(1) Bonosi, F.; Ricciardi, G.; Lelj, F.; Martini, G. *J. Phys. Chem.* **1993**, *97*, 9181.

(2) Markovitsi, D.; Lecuyer, L.; Simon, J. *J. Phys. Chem.* **1991**, *95*, 3620.

(3) Lelj, F.; Morelli, G.; Ricciardi, G.; Roviello, A.; Sirigu, A. *Liq. Cryst.* **1992**, *12*, 941.
(4) Gregg, B. A.; Fox, M. A.; Bard, A. J. *J. Am. Chem. Soc.* **1989**, *111*, 3024.
(5) Morelli, G.; Ricciardi, G.; Roviello, A. *Chem. Phys. Lett.* **1991**, *185*, 486.
(6) Cook, M. J.; Daniel, M. F.; Harrison, K. J.; McKeown, N. B.; Thomson, A. J. *J. Chem. Soc., Chem. Commun.* **1987**, 1148.
(7) McKeown, N. B.; Cook, M. J.; Thomson, A. J.; Harrison, K. J.; Daniel, M. F.; Richardson, R. M.; Roser, S. J. *Thin Solid Films* **1988**, *159*, 469.
(8) Cook, M. J.; McKeown, N. B.; Simmons, J. M.; Thomson, A. J.; Daniel, M. F.; Harrison, K. J.; Richardson, R. M.; Roser, S. J. *J. Mater. Chem.* **1991**, *1*, 121.
(9) Bonosi, F.; Ricciardi, G.; Lelj, F.; Martini, G. *J. Phys. Chem.* **1994**, *98*, 10613.
(10) Clarkson, R. B.; Timken, M. D.; Brown, D. R.; Crookham, H. C.; Belford, R. L. *Chem. Phys. Lett.* **1989**, *163*, 277.
(11) Hankiewicz, J. H.; Stenland, C.; Kevan, L. *Rev. Sci. Instrum.* **1993**, *64*, 2850.
(12) Romanelli, M.; Kurshev, V.; Kevan, L. *Appl. Magn. Reson.* **1994**, *6*, 401.
(13) Mims, W. B. *Phys. Rev.* **1972**, *5B*, 2409; **1972**, *6B*, 3543.
(14) Dikanov, S. A.; Tsvetkov, Yu. D. In *Electron Spin Echo Envelope Modulation Spectroscopy*; CRC Press: Boca Raton, FL, 1992; p 21.
(15) Anderson, M. W.; Kevan, L. *J. Phys. Chem.* **1987**, *91*, 2684.
(16) Kevan, L. In *Time Domain Electron Spin Resonance*; Kevan, L., Schwarz, R. N., Eds.; Wiley: New York, 1979; p 279.
(17) Mims, W. B.; Peisach, J.; Davis, J. L. *J. Chem. Phys.* **1977**, *66*, 5536.
(18) Klauder, J. R.; Anderson, P. W. *Phys. Rev.* **1962**, *125*, 912.
(19) Mims, W. B. *Phys. Rev.* **1968**, *168*, 370.
(20) Gerfen, G. J.; Singel, D. J. *J. Chem. Phys.* **1994**, *100*, 4127.
(21) Berkovitch-Yellin, Z.; Ellis, D. E. *J. Am. Chem. Soc.* **1981**, *103*, 6066.
(22) Bertini, I.; Martini, G.; Luchinat, C. In *Handbook of Electron Spin Resonance*; Poole, C. P.; Farach, H. A., Eds.; AIP Press: New York, 1994; pp 62–65.
(23) Dzuba, S. A.; Raitsimring, A. M.; Tsvetkov, Yu. D. *J. Magn. Reeson.* **1980**, *40*, 83.
(24) Atkins, P. W. *Mol. Phys.* **1967**, *12*, 201.
(25) Kivelson, D. J. *J. Chem. Phys.* **1966**, *45*, 1324.
(26) Kask, N. E.; Kornienko, L. S.; Mandel'shtam, T. S.; Prokhorov, A. M. *Fiz. Tved. Tela* **1963**, *5*, 2306.
(27) Salikhov, K. M.; Dzuba, S. A.; Raitsimring, A. M. *J. Magn. Reson.* **1982**, *42*, 255.

JP9510958